Hypersonics Waveriders Optimized for High Altitude Deployment and Gliding

Varun Unnithan, Duncan Kuchar, Matthew Chou, and Sophie Jack
Advised by: Dr. Christoph Brehm and John Jessen

Despite recent surges of interest, hypersonic flight presents significant challenges due to the lift-to-drag (L/D) ratio barrier. As vehicles become supersonic, their aerodynamic performance decreases, contributing to L/D losses. One promising solution is a waverider, a vehicle that leverages its own geometry and that of its shockwave to create a higher lower body pressure and an increase in its L/D ratio.

This paper seeks to optimize the glide distance of a hypersonic waverider deployed at 40 kilometers, traveling with a horizontal velocity of Mach 10. For this study, the Earth's curvature is neglected, standard atmospheric tables are used, inviscid flow models are used, and perfect gas models are assumed. The geometry of the waverider does not include control systems so control pitching is considered to occur automatically and instantaneously in trajectory optimization. While these assumptions simplify the study, a conversation on their validity and implications takes place.

On a high level, Bayesian optimization was used to iteratively converge upon an optimal waverider geometry. A simple waverider was used as an initial geometry, with seven input parameters corresponding to a given waverider geometry. These input parameters were processed with a meshing script into a VTK file for computational fluid dynamics (CFD) analysis. Once a CFD run was completed and the lift and drag values were processed, the Bayesian optimization process would define a new list of seven input parameters and equivalent waverider geometry, following an expected improvement (EI) metric. This loop would continue until a predefined number of evaluations was completed. This study concludes with a discussion on the optimized resulting trajectories and total glide distance traveled.

I. Introduction

In the 21st century, hypersonic flight systems have seen a steady surge in interest. Competing national interests, commercialized reentry and ascent space systems, and the challenge of achieving fast, long-range transportation systems are all driving forces behind this movement. Most recently, the U.S. and China have entered a new hypersonics race, with both countries devoting significant resources to investigating the hypersonics envelope. On the astronautic side, the commercialization of reentry and ascent vehicles such as SpaceX's Starship, Rocket Lab's Electron Rocket and Blue Origin's New Glenn has significantly pushed research into heat shielding, hypersonic propulsion systems, and e□cient reentry pathing. Meanwhile, in commercial aeronautics, companies such as Venus, Hermeus, and China's Space Transportation are seeking to commercialize high speed air travel. These initiatives advance the national defense, commercialized spaceflight, and high-speed global travel. This cumulative interest underscores the importance of developing solutions in the hypersonic realm.

One of the main challenges to hypersonic flight is overcoming the "L/D" barrier, or the low lift-to-drag ratios present in hypersonic flight, speeds at and above Mach 5. This ratio characterizes a vehicle's e□ciency, particularly the amount of energy needed to keep the system in flight. Vehicles with a high L/D ratio are generally better optimized for glide distance, fuel usage, flight time, and reduced heating with the aerostructures. For general reference, subsonic flight vehicles generally have a max L/D ratio from 13-20 while hypersonic transportation vehicles may cap at 6 [1].

The decreased performance at hypersonic speeds compared to supersonic and subsonic flow is primarily due to intense shock waves and viscous flow e□ects which induce intense drag along the vehicle body. While some vehicle systems, such as orbital reentry capsules, may want to take advantage of these conditions, achieving a high L/D ratio is critical for the other majority of hypersonic vehicles such as cruise missiles, glide vehicles, scramjets, ramjets, and more which optimize for flight distance, time, fuel e□ciency, etc. Therefore, integrating aerodynamic designs which incorporate high L/D ratios is imperative for the future of hypersonic flight.

One solution for achieving higher L/D ratios in hypersonic flight is the hypersonic waverider. These vehicles are designed to generate a shock wave at their nose and ride the wave that propagates along the underbelly of the vehicle. This is done by careful analysis of the resulting shock formations and manufacturing the underbelly of the vehicle to maintain close alignment with the shock wave. This phenomenon, known as compression lift, takes advantage of the increased pressure under a vehicle to create lift and minimize drag. This is analogous to wave-riding in boats where boats are shaped to harness hydrodynamic lift instead of buoyancy for maintaining afloat. While there are several wave rider designs that appear v-tapered or conically derived, the paper's design is defined polynomially.

II. Scientific Design

The novelty of a waverider is that it uses the shock waves generated from its flight to increase its L/D while supersonic. Developed by Terence Nonweiler of the Queen's University of Belfast in 1951, the design of the waverider was first conceived as a re-entry vehicle with a delta-wing platform and low wing loading as shown in Figure 1. From 2010 to 2013, Boeing's unmanned X-51 Waverider demonstrated the application of a hypersonic waverider. The X-51's successful test flight brought about further research and optimization in Nonweiler's concept of the waverider.

This paper explores the optimization of a waverider with various simplifying assumptions. It is first important to define what optimization means in the context of waverider geometry. To optimize the waverider design is to generate as high of a lift-to-drag ratio as possible, while maintaining a body geometry that can be described parametrically. To achieve this, several preceding, more comprehensive works were analyzed and taken into consideration for this paper's waverider design. Such work and its impact on this paper's design is discussed below.

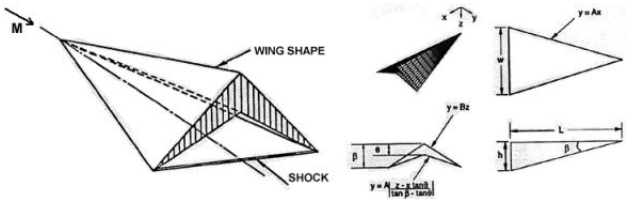

Fig. 1 Nonweiler caret design.

The 2024 paper from the Technical University of Crete titled Design and Evaluation of a Hypersonic Waverider Vehicle Using DSMC employed an equation-based methodology in optimizing the waverider design [2]. The use of two equations, a base curve and a curved section equation, allowed for the authors to trace the streamlines from the conical shock and generate the compression surface geometry. The equation-based approach for geometry optimization was used in this paper.

The initial design for this paper's waverider was drawn from the Nonweiler wing described in the 1986 dissertation by Dr. Kevin Gerald Bowcutt titled Optimization of Hypersonic Waveriders Derived from Cone Flows - Including Viscous E□ects[1]. The Nonweiler wing is a caret-shaped cross section and a delta planform. This general geometry was parameterized for optimization purposes using the following technique.

Gradient-based optimization methods are algorithms that find the minimum or maximum of a function by using the gradient of the function at the current state. In this paper, a gradient-based optimization method was used to find the minimum of the cost function defined by the waverider's geometry equations and the cost of the trajectory. Many methods exist, and the one chosen was Bayesian optimization. The 2018 paper by Peter Frazier from Cornell University titled, A Tutorial on Bayesian Optimization, outlines the method's approach to optimizing objective functions and how to implement such an algorithm [3]. This paper's Bayesian Optimization techniques are based upon the BayesOpt method described in Frazier's work.

III. Problem Statement

Initial conditions are provided to establish operational parameters and a uniform baseline for comparison with similar studies within a similar aerodynamic regime. As previously mentioned, the waverider's initial vertical velocity is 0 m/s and its horizontal velocity is Mach 10. The design dimensions for the waverider are noticeably smaller than what would be practical for any significant design - its length is constrained to 1 m, volume to 1 m^3, and density to 2500 kg/m^3 which yields a total mass of 25 kg. The flow is assumed to be inviscid and the constituent gas molecules are considered ideal. Additionally, as the waverider geometry has no attitude control mechanisms, it is assumed to have the capability to instantaneously control its pitch despite lacking the actual control architecture to do so. Finally, it should be noted that in the CFD program, Zaratan encounters singularities when calculating the pressure alongside the rear of the waverider geometries. For values along the back face, $\frac{P_\infty}{M_\infty}$ is assumed.

While ideal gas modeling and atmospheric tables assumptions are common among preliminary design studies,

there are several assumptions that may be considered over-idealized and problematic. Among the most significant assumptions is instantaneous pitch control. It can be pointed out that assuming such attitude control is impractical with regards to aerostructure loads, pitch actuation systems, and limitations to real world systems. Real systems include error, whether from onboard sensors, vehicle calculations, pilot mismanagement, etc. While this may be the case, pitch control is neglected to avoid the complexity in solving for stability moments. If the focus of this study were on pitch control, it is expected that further shock modeling and mesh refinement will be necessary around the attitude control system. This would be especially important if attitude control mechanisms were located adjacent to the rear face.

The second problematic assumption is solving for an inviscid flow. Although viscous flow is the second overall contributor to vehicle drag, this simplification is necessary to streamline the study's CFD modeling, optimization program's runtime, and fit the time constraints of the project's troubleshooting windows. While realistic models would account for wall shear, weak and strong viscous forces, and slip flow e□ects, these factors are unnecessary when considering the project's nature, an undergraduate capstone project and a preliminary design study [4]. With that aside, wave rider designs incorporating viscous e□ects have been proposed and studied since 1987. These designs, viscous waveriders, have been optimized for skin friction drag and shock drag by modeling the under and upper surfaces with respect to inviscid flow and adding the viscous e□ects as the integral of the boundary layer equations [5]. This may be a useful reference for secondary research investigating such conditions.

The rear pressure assumptions in this study were necessary to provide a baseline model to work with. While assuming $\frac{P_\infty}{M_\infty}$ may not capture the specific aerodynamic flow traveling in the wake or near the rear surface of the waverider, it is a necessary assumption given the significant computational challenges such modeling implies.

IV. High-Level Optimization Path

The general logic path for this project follows the flow chart as show in Figure 2. On a high level end, there is an initial geometry that is then plugged into the Optimization Loop. From here, an optimized geometry is output and an in-depth CFD analysis is run from with a more detailed trajectory analysis.

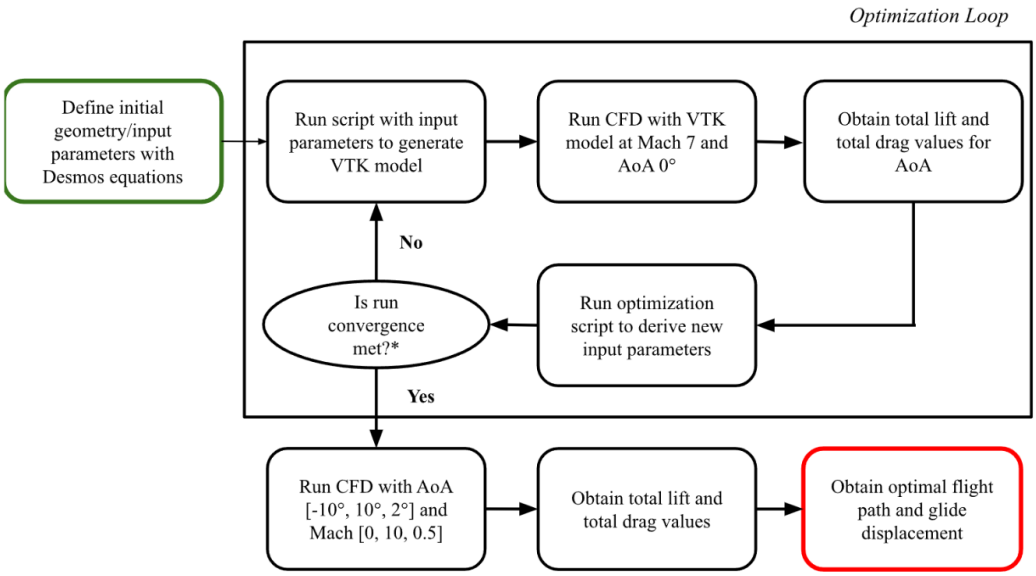

Fig. 2 Optimization process with optimization loop highlighted.

A. Geometry

On a high level, a preliminary geometry is calculated and visualized using Desmos. This geometry consists of several surfaces bounded by seven input parameters or seven degrees of freedom. For the first geometry, initial parameters corresponding to a "ramping" wedge are defined. One of the limitations for seven degree-of-freedom (DoF) modeling was issues of manually tuning the variables to get the given geometry. A true wedge was not definable. These initial parameters are processed through a VTK script, whose specifics are explained further, but whose output is a processable

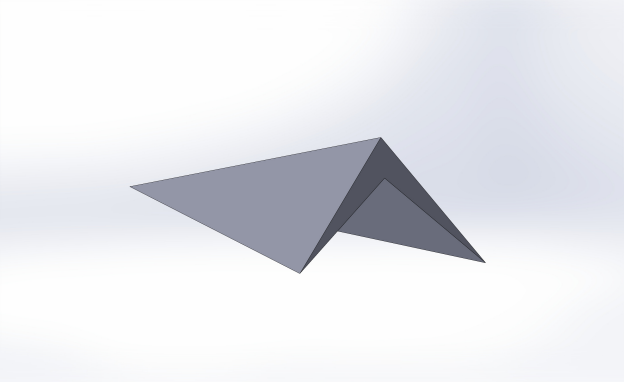

Fig. 3 Angled view of first waverider design

Fig. 4 Back view of first waverider design

VTK file.

B. Zaratan HPC Cluster

The Zaratan High Performing Computing (HPC) Cluster is the University of Maryland's flagship computer designed for high intensity workloads, including Computational Fluid Dynamics. All CFD models and analysis were carried out with HPC's hardware.

C. CFD Assumptions

The VTK file is queued into Zaratan's file list. Several assumptions are made when running the CFD. First, the simulation runs at Mach 7. This is the hypothesized speed over which the waverider is assumed to travel the farthest distance. Additionally, each CFD is run with a waverider at an angle of attack of 0°. This is hypothesized to favor cambered waveriders in the optimization script. These assumptions are made to reduce CFD runtime and post analysis processing. A secondary assumption is made where waverider performance across various geometries increases symmetrically across Mach number and angle of attack. Ideally, a sweep of various Mach numbers and angles of attack would be run on the HPC for a greater characterization of each model but this was a necessary shortcut for basic cost analysis, so only a full sweep was carried out across the final geometry.

D. Optimization Script

The optimization script processes the CFDs' outputs, which are total lift and total drag. Since a total trajectory study would be computationally intensive, this study optimizes for L/D which is an initial proxy for total distance traveled. An optimized trajectory is calculated only after the final geometry has been converged. Convergence is defined when the total number of iterations reaches 1000. If convergence has not occurred, the weights of each surface input parameter are redefined according to the Bayesian optimizer model, whose mathematical details are provided later. Once converged, a greater CFD analysis, with angles of attack swept from -10° to 10° at 2° increments and Mach swept from 0 to 10 at 0.5 increments, and trajectory analysis are processed.

V. Equation-Based Methodology

The first attempt at the waverider geometry was an STL file generated from SolidWorks. After initial research on waveriders, it was determined that the Nonweiler/caret geometry was best for a first design and CFD analysis. The CAD and CFD results are shown in Figures 3 and 4.

This initial attempt using the CAD to CFD workflow revealed that this process was not the most e□cient. To generate the most optimal geometry, many iterations needed to take place, something that the CAD to CFD workflow would not allow for. So, a more automated, code-based approach was taken by parameterizing the geometry via equations.

As mentioned in the Scientific Design section, an equation-based methodology approach was taken for optimizing the waverider's geometry. The graphing calculator web application Desmos was used to generate a 3D visual of the geometry using three equations: one for the top surface, one for the bottom surface, and one for the back surface. These

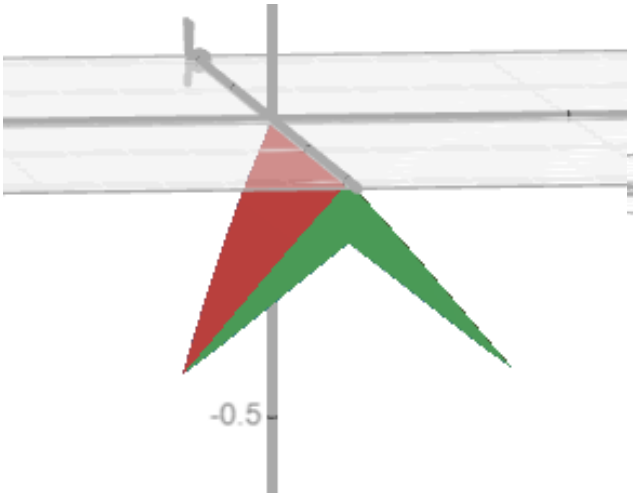

Fig. 5 Angled view of a Desmos geometry

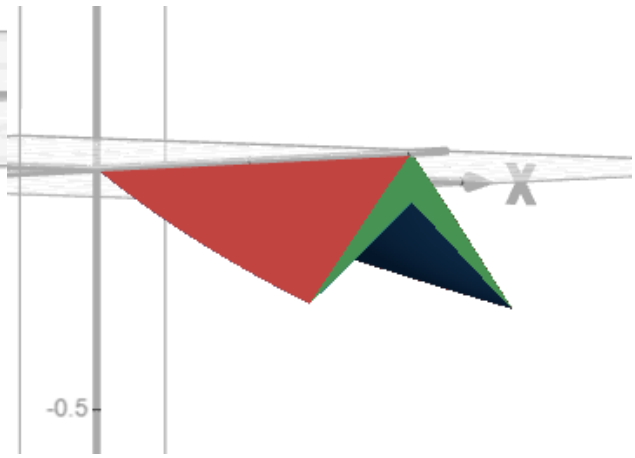

Fig. 6 Back view of a Desmos geometry

equations are listed below, respectively

$$z = ax^4 + cx^2 + g|x|, -1 < y < -qx^2 - s|x| \tag{1}$$

$$z = ax^4 + cx^2 + g|x| + (y + qx^2 + s|x|)(hx^2 - iy + j), -1 < y < -qx^2 - s|x| \tag{2}$$

$$y = -1, ax^4 + cx^2 + g|x| + (y + qx^2 + s|x|)(hx^2 - iy + j) < z < ax^4 + cx^2 + g|x| \tag{3}$$

where x, y, and z are the variables associated with the three dimensions and a, c, g, h, i, j, q, and s are the defining parameters of the geometry. Equation 1 is for the top surface, Equation 2 is for the bottom surface, and 3 is for the back surface of the waverider. Across the three equations, there are eight di□erent variables whose value can be adjusted to manipulate the waverider's geometry. Figures 5 and 6 show an example of an output Desmos geometry.

Another defining equation for the waverider geometry is the volume constraint equation. The constraint of volume to 0.01 m^2 was considered when using finding a geometry with Equations 1, 2, and 3. To ensure the design that was constructed satisfied this volume constraint, the function defining the geometry was integrated. That is, Equation 4 shows the integral that was used to compute and maintain the required volume.

$$\int_{x=0}^{x=\frac{-\sqrt{s^2+4q}}{2q}} \int_{y=-1}^{y=-qx^2-sx} -2(y + qx^2 + sx)(hx^2 - iy + j)\, dx = 0.01 \tag{4}$$

With the Desmos geometry and volume constraint equations, the waverider was parametrized and able to be optimized by manipulating its variable values.

VI. VTK Generation

Instead of manually meshing each geometry, the code has a meshing capability that outputs a VTK file for the CFD to take in. This method takes in the eight parameters that define the geometry equations as discussed in Section V. By defining the geometry equations with these parameters, the waverider can be expressed as a function of x and y in the XY plane. The top and bottom surfaces of the waverider then have points projected onto them from the XY plane.

Initially, the points that will define the mesh of the waverider are defined in the XY plane. The point spacing is dependent on the cosine of the distance to a critical x position, with these positions being $x = 0$, the maximum x value, and the minimum x value. This technique of using the cosine function to condense points around 0, minimum, and maximum x values is called cosine spacing [6]. For the y axis, the mesh resolution determines how many divisions there are. The point $y = 0$ is set as the nose of the waverider. As y decreases from 0 to -1 (moving down the waverider body), there is a linearly increasing point resolution on each y axis division line. For example, the first division line, which is the nose, would have one point, the second division line would have three points, the third division line would

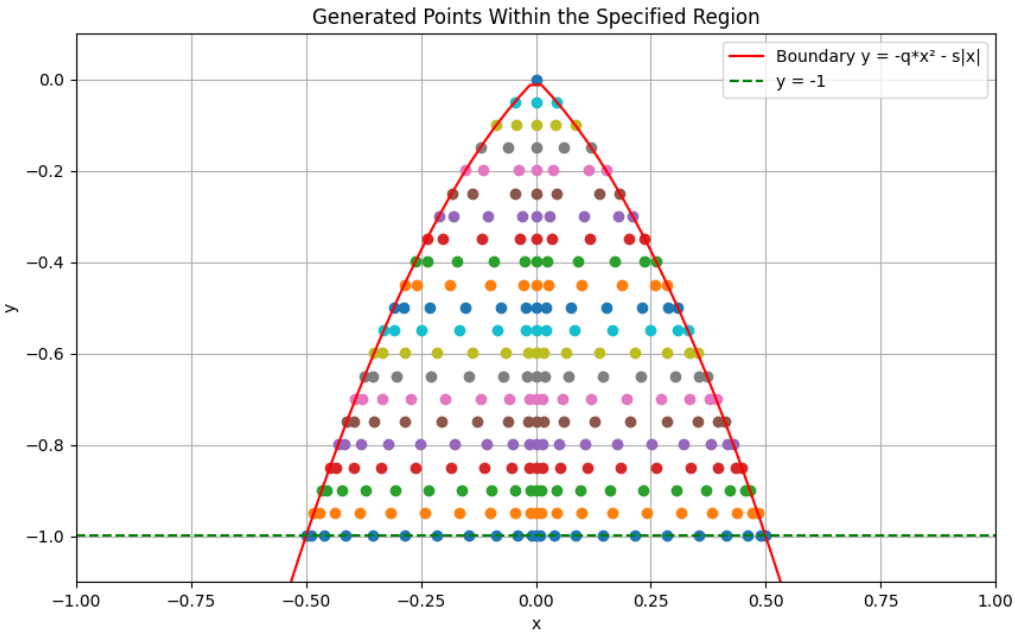

Fig. 7 Points generated in the XY plane

have four points. After the nose, there is always a point on each boundary of the surface, then a linearly increasing amount of points in between the two boundary points. Figure 7 shows an example point map of a waverider geometry.

To create a mesh from this point map in the XY plane, the points are projected on the top and bottom surfaces of the waverider. Figure 8 shows the points projected onto the 3D waverider geometry. From these projected points, triangles are made by connecting points on neighboring y axis division lines to one another. Figure 9 shows the triangular mesh projected onto the waverider geometry.

Each triangle has an annotation attached to it that's the distance from the bottom left corner of the geometry to either x_{max} or x_{min}. These distances are stored so when the volume mesh is being made, it can be determined which cell is close to the boundary. The mesh is then made to be more refined around these boundary points. There is a threshold set to classify points as boundary points. If the stored distances from the bottom left corner to xx_{max} or x_{min} are less than these defined threshold values, then they are used as boundary points, and the mesh is made to be more refined. With the top and bottom surfaces meshed, the back surface of the waverider is made by connecting the two defined upper and lower surfaces. The back surface is meshed using the same triangular meshing scheme as before, but now with only two division lines.

VII. Geometry Optimization and Trajectory Search

There are two aspects of the waverider that must be considered when maximizing its distance traveled: its geometry and its trajectory. So, two optimization loops were employed to explore both characteristics of the waverider. The geometry optimization loop is optimizing lift/drag (L/D) by massaging the geometry parameters of the waverider, while the trajectory search algorithm maximizes distance traveled by varying a function representing the angle of attack of the waverider throughout the flight as a function of distance.

First, a geometry optimization loop takes in the eight parameters of the waverider's geometry, as discussed in Section V. Using the volume constraint integral shown in Equation 4, any parameter can be solved for, turning the 8 DoF system into a 7 DoF system. The parameter i was chosen to be solved for because it returns the least complex set of constraints. Now, seven varying parameters and one constant parameter are used in the geometry optimization loop.

In this optimization loop, the CFD is being called and run each iteration. The geometry parameters from the above discussion are used to create a mesh that is taken in by the CFD. Lift and drag values from the CFD are used to get the

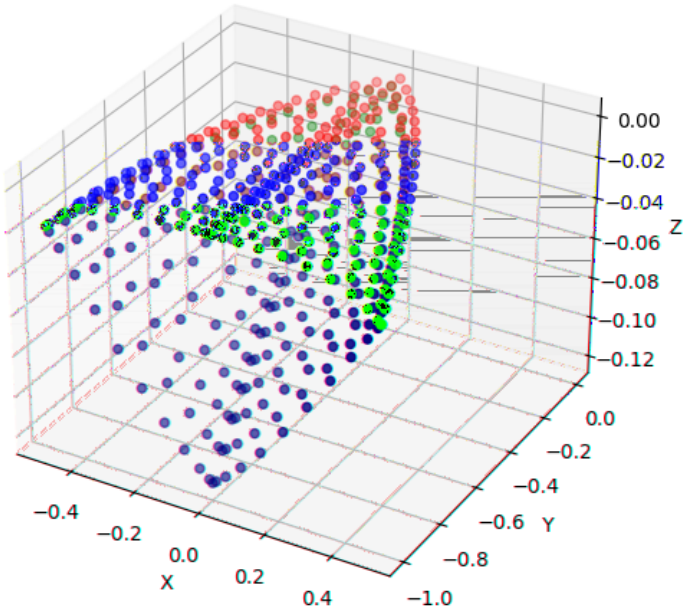

Fig. 8 Points from the XY plane projected onto 3D waverider geometry

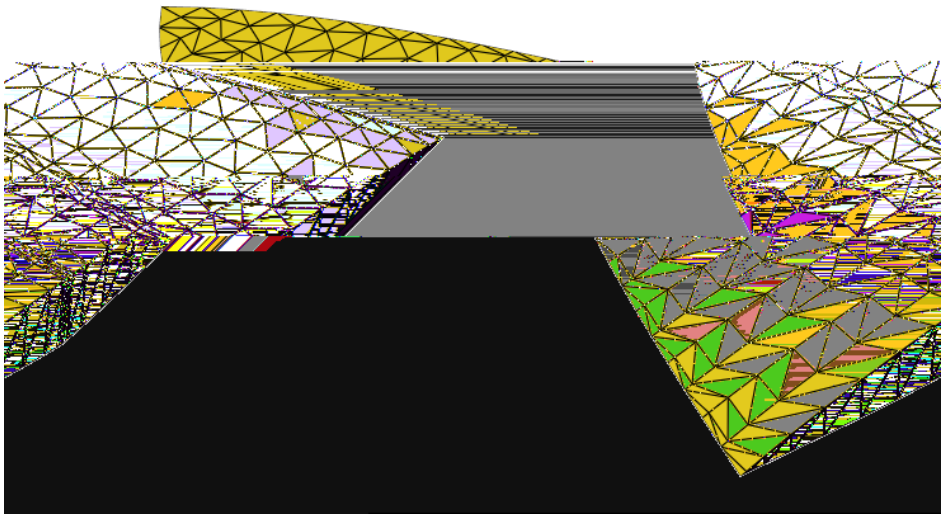

Fig. 9 Triangular meshing on a waverider geometry

lift and drag coe□cients of the waverider. Back pressure, as mentioned in Section III, is computed as $\frac{p_\infty}{M_\infty}$, taken at an altitude of 30 kilometers and Mach 7. So, force due to back pressure is computed via

$$F_b = A_b \frac{p_\infty}{M_\infty} \tag{5}$$

where A_b is the area of the back surface of the waverider. This force due to back pressure is considered in computing

L/D.The CFD output does not consider back pressure, so the computed force due to back pressure from Equation 5 must be subtracted from the drag output by the CFD. So, L/D is computed as

$$\frac{F_L}{F_D} = \frac{F_{L_{CFD}}}{F_{D_{CFD}} - F_b} \tag{6}$$

where $F_{L_{CFD}}$ is lift force from the CFD, $F_{D_{CFD}}$ is the drag force from the CFD, and F_b is the force due to back pressure from Equation 5.

The lift/drag value from Equation 6 is multiplied by a scaling factor, since lift is typically relatively small. Bayesian Optimization is used to optimize this scaled L/D. An important note is that L/D is taken as the negative value, since Bayesian Optimization aims to minimize the output by manipulating the parameters.

Bayesian Optimization was chosen for this optimization loop over other gradient-based optimization methods, like Nelder-Mead and Constrained Optimization by Linear Approximation (COBYLA) for several reasons. Methods including and similar to Nelder-Mead and COBYLA were not chosen because they are less optimal when you have a restricted number of evaluations, since they typically run to convergence of a solution. These methods are more likely to become trapped in a local minima, or suboptimal solutions, compared to Bayesian optimization, which can run on a predefined number of evaluations. This can better balance exploration and exploitation. Bayesian optimization also models the system statistically, so confidence metrics can be extracted from it.

A notable feature of the Bayesian Optimization algorithm is that the penalization is proportional to how far the generated volume is to the constraint volume of 0.01 m^3. So, the further the generated volume for a given evaluation is, the larger the penalization for it. This ensures that the optimization process generates as many geometries as possible with the correct constraint volume.

The second optimization loop is a trajectory search algorithm. This loop takes in six parameters that define a damping oscillation equation, given by

$$AoA(x) = \frac{A}{(x-c)^n} \cos\left(b(x-c)\right) + k(x-c) + d \tag{7}$$

where A, b, c, d, k, and n are the six parameters of the damping oscillation equation.

This damping oscillation equation is taken as the angle of attack (AoA) function, which is a function of distance. This AoA function is taken as the cost function to a Nelder-Mead optimization method algorithm. Within this algorithm, the trajectory of and distance traveled by the waverider is determined.

It uses L/D from the previous optimization loop and AoA from the AoA function to create the equations of motion of the waverider. The distance traveled by the waverider is then found by propagating the current state of the waverider by forward integrating its equations of motion. The distance traveled is the cost of the function, and Nelder-Mead aims to minimize the negative of the distance, therefore maximizing distance traveled by the waverider. It does this by determining a new set of parameters for the damping oscillation equation based on the previous iterations. This closes the optimization loop of the trajectory search algorithm.

VIII. CFD

A. CFD Overview

Computational Fluid Dynamics (CFD) is a branch of fluid mechanics used for analyzing fluid behavior and their interactions with surfaces. CFD simulates flow conditions and predicts vehicle flight performance by analyzing a mesh, a model of cells with each cell representing a discrete point where aerodynamic equations are solved. Here, an increase in cell size inversely a□ects the resolution of the mesh and the accuracy of the mesh but decreases the time cost to run the CFD. Since models contain millions of cells, it is important to strategically define the density of cells around a vehicle's points of interest. Typically, cell density decreases away from the model and becomes higher as the vehicle surface gets closer. This study employs an optimization learning model that converges upon a high L/D waverider geometry after 1,000 CFD runs. Since each run can take two to twenty minutes and the waverider's geometry is entirely derived from CFD results, optimizing time cost is essential for e□ciency and practical design iterating. One way to optimize time cost is to run a mesh independence study, which evaluates analytical convergence as a function of cell count and cell size. A mesh independence study was performed on seven cases, ranging from 300,000 cells to 55 million cells, to evaluate the relationship between cell density and computational e□ciency. A case independence study was conducted to verify the time required for analytical convergence and flow field stabilization with respect to a number of

time steps. The mesh independence study established a reliable mesh to standardize across the 1,000 iterations, while the case independence study established a reliable time-step analysis across the 1,000 iterations. Both studies were essential towards minimal computational cost.

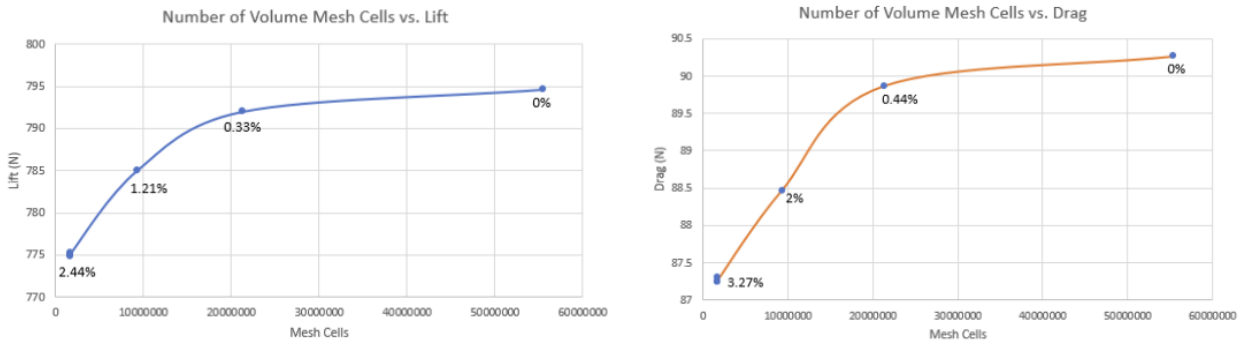

Fig. 10 Mesh refinement performance as a function of cell count

B. Mesh Independence Study

A mesh independence study is essential to determine the optimal balance between mesh resolution, computational cost, and reliable analytical results. This section evaluates the convergence behaviors of various meshes, referred to as cases, by comparing their analytical solutions to a reference mesh, a mesh which has the highest cell count and is assumed to represent real world flow conditions. Each mesh is characterized by the number of cells and cell size contained, with larger numbers of cells and smaller cell size corresponding to greater resolution. A focus on regions of high flow complexity - points closer to the body, points experiencing flow transition, or surface edges - is crucial for successful CFD resolution and analysis. The goal of a mesh study is to ensure that a mesh with lower computational cost has comparable results to the reference mesh, deemed statistically significant at 5% deviation. The reference mesh, established in 1, contains approximately 55 million cells, seen in 14, and analytically evaluates to a total lift force of 794.632 N and total drag force of 90.2687 N. To resolve the best computational mesh, six comparison cases, ranging in total cell count and cell density, were investigated.

Cases 1-3 were all similar to each other. They had the lowest computationally intensive meshes, seen in 13, that were considered viable for the optimization script. These cases contained 3% of the reference case's cells and maintained an error margin of 2-3% with respect to reference lift and drag in 10. While pressure spikes were observed in these cases, they were considered insignificant in influencing waverider geometry 11. Cases 4 and 6 were transition cases towards the reference case, exhibiting small errors of 2.5% and 0.4% respectively, in 10. The cases provided insight in bridging mesh performances between the lower computationally intensive meshes and the reference case. Case 7 was the least refined mesh and displayed extreme pressure spikes that were significant to influence the waverider geometry in 12. This case defined the lower boundary of mesh viability. Based on the data, Case 1 was selected for the optimization script due to its fast runtime and close agreement with the reference case lift and drag values.

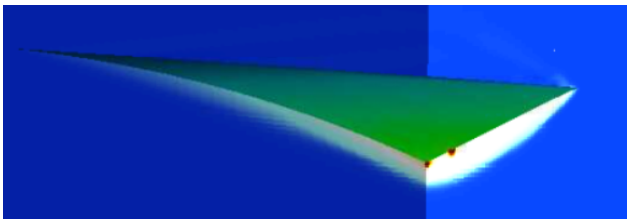

Fig. 11 Pressure spikes visible on Case 1

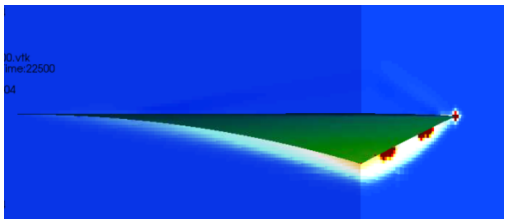

Fig. 12 Pressure spikes visible on Case 7

Case	Number of Cells	Lift (N)	Drag (N)	Cell Size	Surface Distance	% Lift Error from Max Precision Case	% Drag Error from Max Precision Case
1	1670656	775.274	87.3142	0.004	0.001	2.4361	3.273
2	1670656	774.874	87.2536	0.004	0.01	2.486	3.3401
3	1675264	775.049	87.2501	0.004	0.05	2.4644	3.344
4	9304064	784.982	88.4675	0.002	0.05	1.2144	1.995
5	55428608	794.632	90.2687	0.001	0.05	0.00	0.00
6	21319168	792.005	89.8697	0.004	0.001	0.3306	0.4420

Table 1 Case parameters and analytical solutions

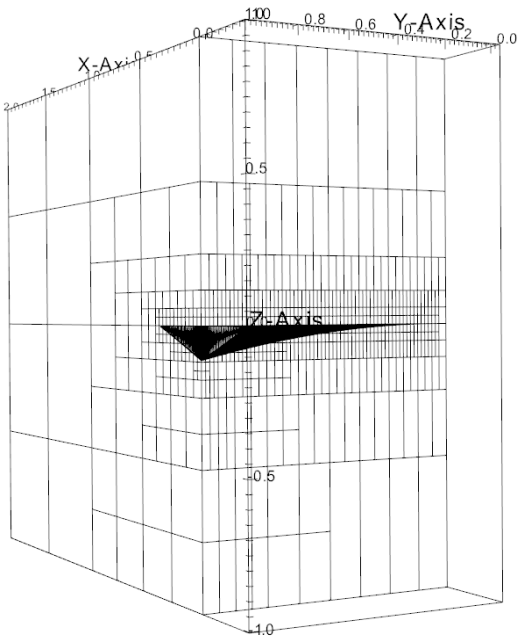

Fig. 13 Case 1's refinement mesh

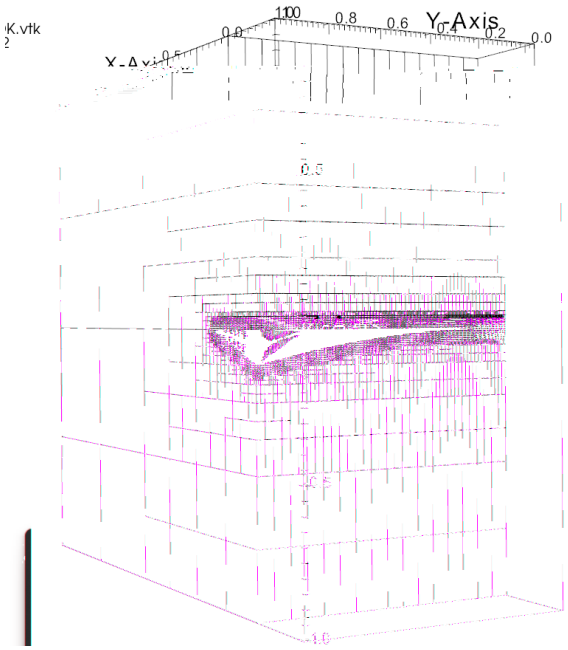

Fig. 14 Case 5's refinement mesh

1. Volume Meshing

The surface mesh is provided in a VTK file, a file compatible with the CFD program. The VTK file defines the geometry through a list of points in space and triangular elements, defined by their indices corresponding to the list of previously described points. The VTK serves as the framework around which the volume mesh can be defined. The volume mesh defines the cells surrounding the surface mesh, which represents the waverider. To generate the volume mesh, cells are given a resolution size and a vertical distance from the surface mesh. For the best-case scenario, a cell size of 0.001 and a refinement distance of 0.05 were used to capture flow fields. Away from the surface, larger cells were used to reduce computation cost. A blending region ensures a gradual transition between these fine and rough cell regions. For all cases, cells were square-shaped. The various cell sizes and refinement distances are summarized below.

C. Case Independence Study

A case independence study evaluates the e□ects of various parameters on the analytical results of the CFD run. This study specifically evaluates the e□ect of time-steps with regards to Large Eddy Simulation (LES) techniques, specifically Wall-Modeled Large Eddy Simulation (WMLES), a method of CFD analysis that combines the accuracy of numerically solving the Navier-Stokes Equations while also maintaining computational e□ciency with flow approximation. The

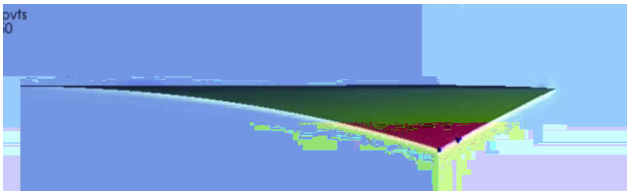

Fig. 15 Flow field at time-step = 50

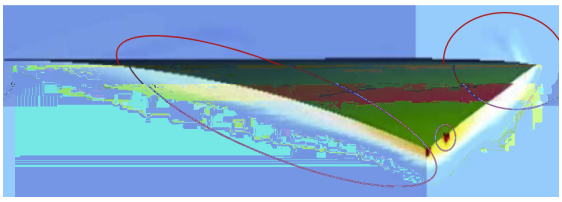

Fig. 16 Flow field at time-step = 250

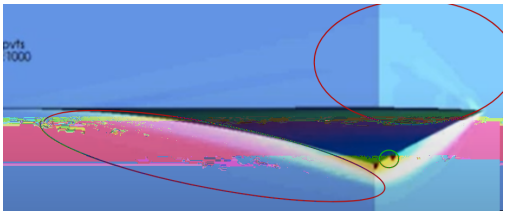

Fig. 17 Flow field at convergence, time-step = 1000

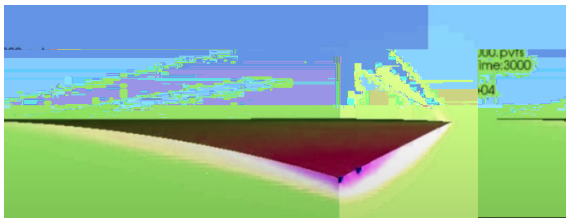

Fig. 18 Flow field with safety factor, time-step = 3000

Cartesian Higher-order Adaptive Multi-Physic Solver, better known as CHAMPS, operates at a default 22,000 calculable time-steps, where each time step represents an incremental progression in flow simulation. To resolve the flow conditions, CHAMPS simulates flow far ahead of the surface mesh, iterating forward for each time-step resolved. At each time-step the flow in each cell is resolved, and as the simulation progresses, the flow-field is calculated over the entirety of the surface mesh. As this happens, flow features, such as shocks and expansion fans, and analytical solutions, in this case lift and drag, begin to take shape. While CHAMPS can simulate 22,000 time-steps, it is often computationally intensive to undertake. The purpose of this study is to define the minimum time-steps necessary for flow features and analytical solutions to converge. Two primary factors influence CFD complexity, the length of each time step and the total number of time steps. Finer meshes increase the computational cost per time step. Similarly, more complicated geometries increase not only the length of each time step but the total number of time steps needed for convergence. Without convergence, there is no validity to the model so it is critical to balance mesh resolution and time step length. At time-step = 50, there was no flow simulated over the surface mesh 15. For Case 1 mesh conditions, it was observed that lift and drag began to converge at approximately 250 times steps in 16. At this time however, the flow field itself was still developing. Flow field convergence was not achieved until 1,000 time steps in 17. However, to ensure accuracy, a safety factor of three was applied, leading to 3,000 time steps for each CFD run in 18 In the CFD, expansion fans were located along the rear of the waverider and shock waves were observed along the underbody of the vehicle.

IX. Results

Out of the 1000 iterations conducted, only 61 iterations contained valid geometries. While this was predicted in the code output, it was still a surprise for the Bayesian Optimizer. Several of these geometries are presented in increasing L/D performance in 19 and 20. The Bayesian Optimizer, which iterates over the seven surface parameters, is seen to explore unconventional configurations, demonstrating its ability to explore and exploit its optimization variables.

The most optimal geometry identified was a waverider with a triangular top view and ramped side view, seen in 21 and 22. It is important to note that this is technically not a waverider due to its geometry deriving from L/D optimization and not with classical projected shock considerations. Additionally, due to time constraints, there was not su□cient time to sweep along Mach number and angle of attack as planned. Therefore, angle of attack optimization was not possible along the waverider's trajectory. When simulating trajectory deployment, seen in 23, the waverider was held at 0° under normal atmospheric conditions.

Upon analysis of the trajectory, it can be seen that the waverider vertically oscillates along its 4900 km horizontal displacement, seen in 23. This behavior arises due to the waverider's geometry, where even at 0° angle of attack, there are conditions where pressure di□erentials and flow conditions can induce positive lift. It can also be seen that the waverider enters free fall at 4900 km horizontal displacement. This is a conservative estimation for the breakdown of the shockwave and induced lift boundary of the waverider. Beyond this point, the code predicts a steady free fall, cutting o□ the distance that the waverider can travel. Additionally, at 4900 km, the waverider code predicts infinite

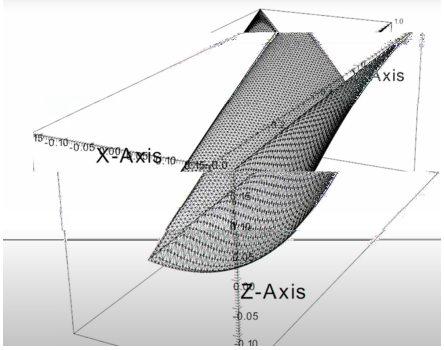

Fig. 19 Exploration of waverider geometry, low L/D

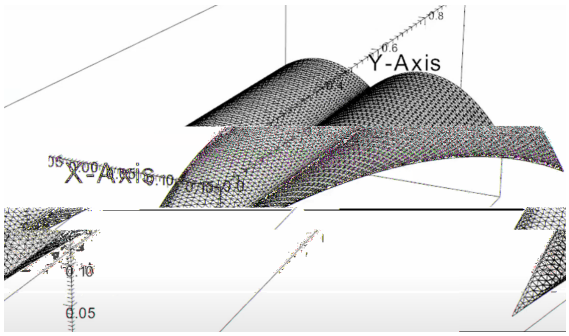

Fig. 20 Exploration of waverider, medium L/D

Fig. 21 Side view of the waverider

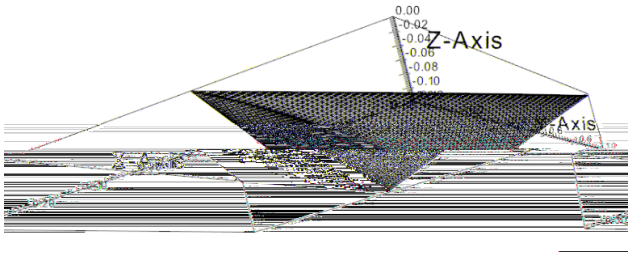

Fig. 22 Isometric view of waverider

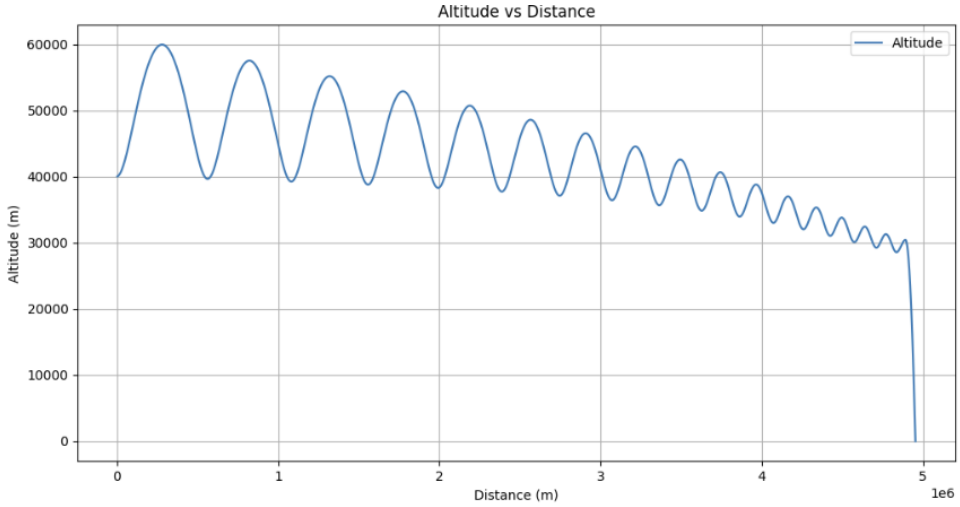

Fig. 23 Mesh refinement performance as a function of cell count

oscillations of the waverider at a steady altitude of 28 km, which identifies a simulation no longer valid. Therefore, the trajectory code cuts o this asymptote and sends the vehicle back down to the surface. Finally, the maximum L/D for the optimized geometry was 8.89 at Mach 7.

X. Conclusions

In conclusion, this preliminary investigation into hypersonic waveriders has demonstrated the use of CFD programs and Bayesian optimization models to enhance geometric design. Although only 61 of 1,000 geometries successfully met the volume criteria, the script demonstrated successful exploratory characteristics associated with Bayesian optimization. In future work, it will be important to explore constrained optimization equations, which although are

more computationally intensive, would provide broader ranges of usable geometry. Furthermore, completing a full CFD-derived trajectory, considering dynamic angles of attack and Mach number will enhance the fidelity and application of this design approach.

References

[1] Bowcutt, K. G., "Optimization of Hypersonic Waveriders Derived from Cone Flows - Including Viscous E□ects," 1986.

[2] Klothakis, A., and Nikolos, I. K., "Design and Evaluation of a Hypersonic Waverider Vehicle Using DSMC," 2024.

[3] Larroque, A., "Variations on Bayesian Optimization Applied to Numerical Flow Simulations," 2018.

[4] Corda, S., and Anderson, J., "Viscous Optimized Hypersonic Waveriders Designed from Axisymmetric Flow Fields," 1988.

[5] Kevin G. Bowcutt, J. D. A., and Capriotti, D., "Viscous Optimized Hypersonic Waveriders," 1987.

[6] Y.M.C. Delaure, A. L., "3D Hydrodynamic Modelling of Fixed Oscillating Water Column Wave Power Plant by a Boundary Element Methods," 2003.